Graphene Oxide Nanosheet Wrapped White-Emissive Conjugated Polymer Nanoparticles

Dong Youn Yoo,[†,‡] Nguyen Dien Kha Tu,[§,¥] Su Jin Lee,[†] Eunji Lee,[∥] Seong-Ran Jeon,[⊥] Sunyong Hwang,[#] Ho Sun Lim,[△] Jong Kyu Kim,[#] Byeong Kwon Ju,[‡] Heesuk Kim,[§,¥,*] and Jung Ah Lim[†,¥,*]

[†]Interface Control Research Center, Future Convergence Research Division, Korea Institute of Science and Technology, Seoul, Korea, [‡]Department of Electrical Engineering, Korea University, Seoul, Korea, [§]Photo-electronic Hybrids Research Center, National Agenda Research Division, Korea Institute of Science and Technology, Seoul, Korea, [∥]Graduate School of Analytical Science and Technology, Chungnam National University, Daejeon, Korea, [⊥]LED Applied Research Center, Korea Photonics Technology Institute, Gwangju, Korea, [#]Department of Material Science and Engineering, Pohang University of Science and Technology (POSTECH), Pohang, Korea, [△]Electronic Materials and Device Research Center, Korea Electronics Technology Institute, Gyeonggi-do, Korea, and [¥]Nano-Materials and Engineering, Korea University of Science and Technology (UST), Dae-Jeon, Korea

ABSTRACT We have demonstrated the preparation of white-emissive conjugated polymer nanoparticles wrapped with graphene oxide (GO) nanosheets. Highly stable, GO-wrapped, poly(9,9-di-*n*-octylfluorenyl-2,7-diyl) nanoparticles (GO-PFO NPs) with diameters in the range 30−150 nm were successfully obtained by utilizing the GO nanosheets as an interface stabilizer in an emulsification process. The synthesized GO-PFO NPs exhibited unique white-emitting photoluminescence with a characteristic green-emissive broad band above 500 nm, which was distinct from the photoluminescent behavior of PFO NPs without GO. This green emission was deduced to originate from the presence of the GO nanosheet shell surrounding the PFO NPs, rather than from luminescence of GO itself or formation of keto defects in the PFO chain. PL decay analysis showed that the GO-wrapped PFO NPs had a longer luminescence lifetime in comparison to PFO NPs without GO, and highly efficient energy transfer to lower energy state induced by the GO occurred.

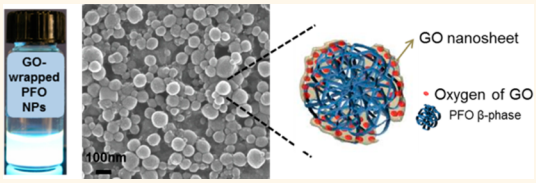

KEYWORDS: conjugated polymer · nanoparticle · graphene oxide · fluorescence · core−shell structure · polyfluorene · green emission

Conjugated polymer nanoparticles (CPNs) are attracting considerable interest in a wide variety of fields owing to their potential for use in applications such as biological labels, chemical sensors, and optoelectronic devices.[1,2] Compared with conjugated polymer thin films, which are commonly prepared by casting from a molecular-dissolved solution, CPNs exhibit superior photostability and light emission efficiency.[3,4] Moreover, CPNs can suppress the undesired energy transfer from high band gap to lower band gap chromophores. This property is especially beneficial for use of CPNs in white-light-emitting devices, which generally consist of a mixture of red-, green-, and blue-light-emitting polymers. However, such devices require careful control of each color contribution to obtain a pure white color. It has been suggested that this issue may be overcome by development of white-emissive CPNs. To date, most such white-emitting nanoparticles that have been developed have been based on organic/inorganic hybrids or doped inorganic nanoparticles.[5−8] However, the reports concerning white-emissive CPNs are rare. Vijayakumar *et al.* reported the preparation of white-emissive organic nanoparticles (NPs) based on an oligofluorene derivative doped with orange-red-emitting dye,[9] while Park *et al.* successfully synthesized white-emitting CPNs consisting of a core−shell structure, with the core emitting blue and the shell emitting green-yellow light.[10]

CPNs are routinely produced *via* a miniemulsion process using an interface stabilizer such as a surfactant.[1,11,12] A miniemulsion is composed of two immiscible liquids (*i.e.*, oil and water) in which micro- or nanosized droplets are dispersed in a continuous phase. They are stabilized by an amphiphilic substance that spontaneously locates at the hydrophilic/hydrophobic boundary interface to lower the interfacial

* Address correspondence to jalim@kist.re.kr, heesukkim@kist.re.kr.

Received for review October 1, 2013 and accepted April 7, 2014.

Published online April 15, 2014
10.1021/nn4050968

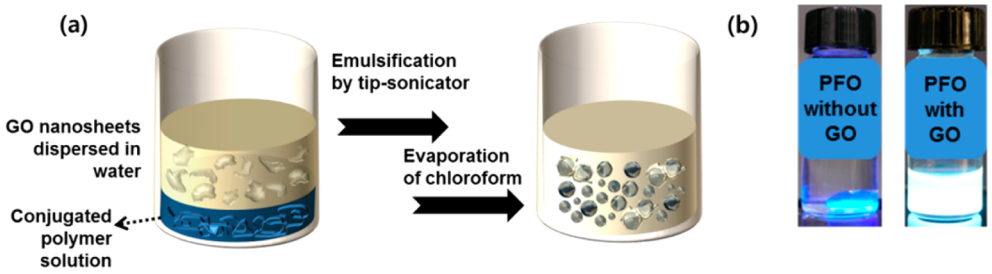

Figure 1. (a) Schematic illustration of the preparation of GO-PFO NPs. (b) Photographs showing PFO emulsions with (left) and without (right) GO sheets in aqueous solution (UV light exposure at 365 nm).

tension. Recently, there has been particular interest in the use of chemically derivatized graphite oxide nanosheets, commonly called graphene oxide (GO), as a two-dimensional molecular surfactant. GO is essentially a graphene sheet functionalized with carboxylic acid groups at its edges, and phenol, hydroxyl, and epoxide groups on the basal plane.[13] Huang and coworkers clearly demonstrated that GO is an amphiphilic substance and can reside at the water/oil interface in a similar way to surfactants. Thus, GO can act as a molecular dispersing agent to produce insoluble materials such as graphite and carbon nanotubes in water.[14] More recently, by using interfacial positioning GO, sulfur-encapsulated reduced GO[15] and graphene-encapsulating nanoparticles[16] have been reported. As a molecular surfactant, GO is fascinating because its oxygen-containing functional groups enable decoration of the material surface with other molecules, producing multifunctional hybrids and composites. The ease of conversion to reduced GO provides a promising method for the fabrication of graphene-hybrid materials such as NPs,[17,18] nanowires,[19,20] or bacteria.[21,22]

In this work, we prepared and characterized white-emissive water-dispersible CPNs wrapped with GO nanosheets. Highly stable nanoparticles composed of poly(9,9-di-*n*-octylfluorenyl-2,7-diyl) (PFO), with diameters in the range 30−150 nm, were formed when single-layered GO nanosheets with small lateral dimensions of approximately 200 nm adsorbed onto the nanoparticle surface to lower the interfacial tension in the emulsification process.

RESULTS AND DISCUSSION

Figure 1a illustrates the preparation of the GO-wrapped PFO NPs. We begin with the formation of an oil/water interface between a chloroform solution of the conjugated polymer and an aqueous dispersion of GO. This two-phase system was then emulsified using a tip sonicator, and the chloroform was then removed by vigorous stirring at 60 °C. Figure 1b shows a photographic comparison of the emulsified solution in the presence and absence of the GO nanosheets. The representative blue-emissive polymer polyfluorene was used as the conjugated polymer in the present study. When the GO nanosheets were added to the aqueous phase, a homogeneous PFO dispersed solution was obtained; by contrast, phase separation due to droplet coalescence occurred in the absence of GO. This indicates that GO nanosheets stabilized the PFO emulsion by adsorption at the interface of the two phases. We found that the obtained GO-PFO aqueous solutions were highly stable for at least 3 months. Figure 1b shows the change in the fluorescence of PFO from blue in chloroform to near white in the GO-wrapped emulsion state under ultraviolet (UV) illumination (λ_{max} = 365 nm). This photoluminescence (PL) behavior will be discussed further below.

Figure 2a shows a scanning electron microscopy (SEM) image of the prepared GO-PFO NPs, where spherical particles of around 30−150 nm in diameter are evident. The GO used to wrap the PFO NPs mainly consisted of single-layer sheets (thickness of GO is approximately 1 nm) with an average lateral size of approximately 160 nm (standard deviation 25%), as shown in Figure S1 of the Supporting Information. The diameter of the GO-PFO NPs determined by dynamic light scattering (DLS) analysis was found to be around 140 nm with a narrow size distribution (polydispersity index = 0.114) (Figure 2b). The larger size identified by the DLS could be due to hydration of the GO shell of PFO NPs in solution, increasing the observed radii in comparison to the dry state of the samples used for SEM imaging.[23] To gain insight into the dispersion of GO-PFO NPs in aqueous solution, the prepared particles were observed using cryogenic transmission electron microscopy (cryo-TEM). As shown in Figure 2c, GO-PFO NPs were effectively stabilized by the GO, forming a sphere shape in aqueous medium. Figure 2d shows selected area electron diffraction (SAED) patterns of GO-PFO NPs with characteristic Bragg diffraction spots, rather than the arc-shaped or ring-type diffraction that is often observed for the nanostructured polymeric materials. In practice, the SAED pattern of PFO nanoparticles prepared in the absence of GO nanosheets exhibited a broad hollow ring, which is attributed to the amorphous carbons from PFO chains, as shown in the inset of Figure 2d. This confirms that the 6-fold symmetry seen in the SAED pattern originates from graphene or graphite, allowing the designation of peaks using Miller−Bravais (*hkl*) indices, with the PFO polymer being amorphous. TEM electron diffraction

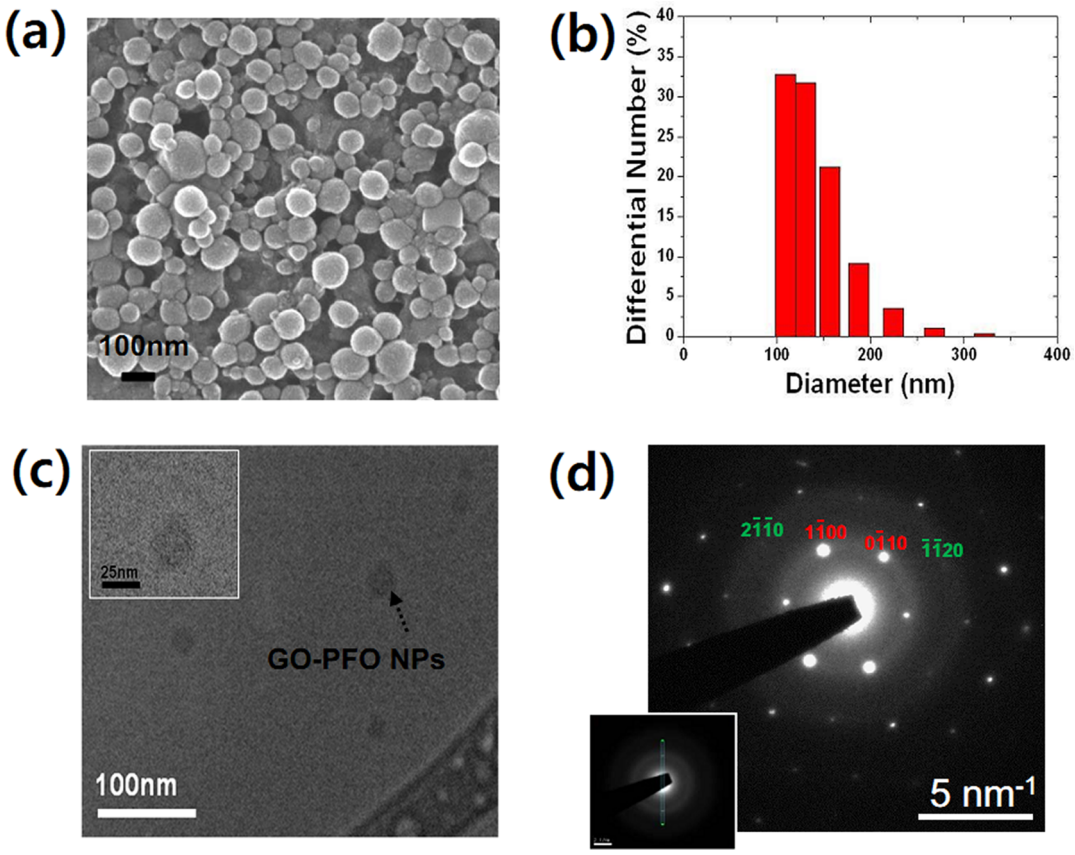

Figure 2. (a) SEM image and (b) DLS histogram of GO-PFO NPs. (c) Cryo-TEM images of GO-PFO NPs (inset: high-magnification image). (d) SAED pattern of a GO-PFO NP from the center of the particle shown in the inset of (c). (The inset shows the SAED pattern of PFO nanoparticles prepared in the absence of GO nanosheets.)

analysis has previously been used to provide definitive identification of GO sheets. Meyer *et al.* reported that the relative intensities of the $1\bar{1}00$ type and $2\bar{1}\bar{1}0$ type reflections, and their behavior with specimen tilt, could be used to distinguish between single-sheet graphene and graphite-like ordered multilayers.[26] For Bernal (AB) stacking of multilayers, the $21\bar{1}0$ reflection spots have been shown to be more intense relative to the $1\bar{1}00$ reflection spots in ED patterns,[25] whereas for a monolayer the $1\bar{1}00$ reflection spots were found to be the more intense. Therefore, higher diffraction intensities for the $1\bar{1}00$ than the $21\bar{1}0$ reflection spots in the SAED pattern of the GO-PFO NPs strongly indicate that monolayer-like GO sheets wrapped around and stabilized the PFO NPs in water.

The morphology of GO–CPNs was influenced by the relative quantities of polymer and GO, in addition to the dimension of the GO nanosheets. With a high quantity of GO relative to that of the conjugated polymer, the nanoparticles became independently wrapped by the GO nanosheets and well dispersed throughout the aqueous phase. In contrast, when only a low amount of GO was used, the nanoparticles aggregated to form clusters of particles (Figure S2). Furthermore, when the GO nanosheets were large, in the range of 500 nm to 1 μm in lateral dimensions, one GO nanosheet tended to encompass several PFO NPs at one time, providing a blanket-like effect where the GO nanosheets had wrinkling around PFO NPs (Figure S3). The individual spherical GO-PFO NPs shown in Figure 2a were prepared using GO nanosheets of around 200 nm in lateral dimension. It is clear that this particular size of GO was appropriate for coating each particle with two or three sheets, providing a well-dispersed suspension. Owing to the nature of GO, this method could be universally used for other CPNs.

To investigate the photophysical properties of the synthesized GO-PFO NPs, UV–vis absorption and PL spectra were acquired. Figure 3a shows normalized absorption and PL spectra of a pristine PFO chloroform solution and an aqueous GO-PFO NP solution. A typical PFO solution exhibited an absorption onset at 420 nm with a single band at 385 nm assigned to the $S_0 \rightarrow S_1$ (0–0) transition of glassy PFO. By comparison, the absorption spectrum of the GO-PFO NP solution was characterized by a main band at 390 nm, which was slightly broader and had a shoulder near 400 nm, and an additional peak at 435 nm.[27,28] The absorption peak at 435 nm was assigned to the $S_0 \rightarrow S_1$ (0–0) transition of the β-phase of PFO. This β-phase represents an isomer planar conformation with an extended conjugation length; therefore, the photophysical properties

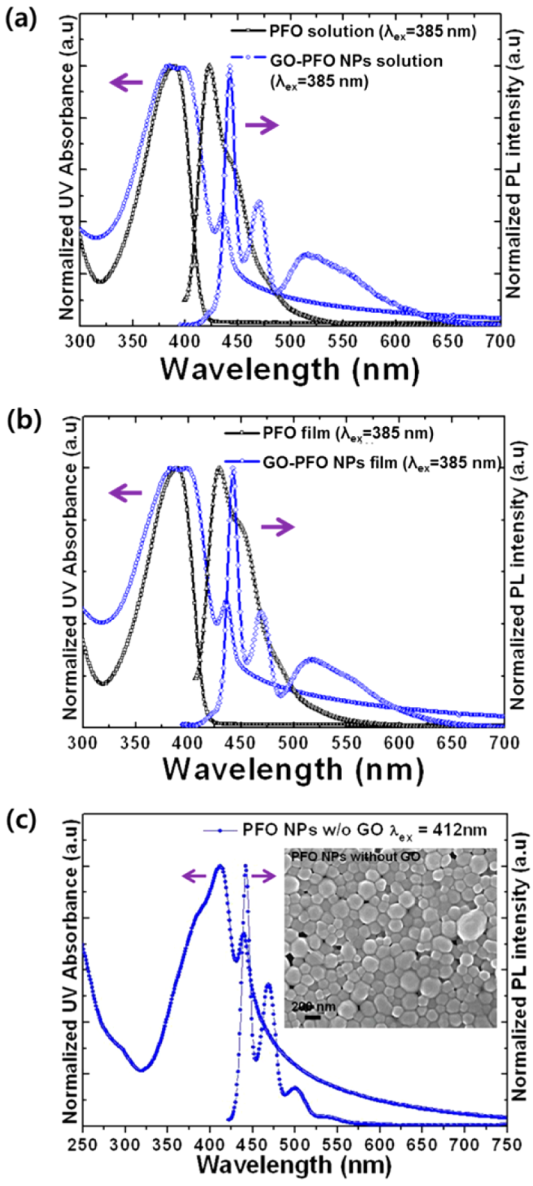

Figure 3. (a) Comparison of UV−vis absorption and PL spectra of pristine PFO and GO-PFO NP solutions and (b) pristine PFO and GO-PFO NP films. (c) UV−vis and PL spectra of PFO NPs prepared without GO nanosheets (inset: SEM image of PFO NPs without GO).

of the β-phase PFO corresponded to a lower energy gap compared to that of the glassy matrix.[28] Its primary photophysics are generally characterized by sharp absorption and emission lines that are red-shifted (>20 nm) with respect to pristine PFO.[29,30] The PL spectrum of the PFO solution can be seen to exhibit a characteristic vibronic progression, with peaks located at 421, 442, 477, and ~503 nm arising from the $S_1 \rightarrow S_0$ (0−0) singlet exciton transition of pristine PFO with (0−1), (0−2), and (0−3) vibronic replicas, respectively. In comparison with the pristine PFO solution, the GO-PFO NP solution exhibited red-shifted and sharp emission peaks at 442 and 468 nm, which were attributed to the $S_1 \rightarrow S_0$ (0−0) and (0−1) transition of β-phase PFO with associated vibronic replicas. This is indicative of a narrowed distribution of emitting PFO chain segments with increased effective conjugation lengths. It is of particular note that a characteristic broad emission band above 515 nm was observed for the GO-PFO NP, which was mainly responsible for the white emission of these particles.

Figure 3b shows a comparison of absorption and PL properties of films consisting of pristine PFO and GO-PFO NPs. In the PL spectrum of the pristine PFO film, characteristic vibronic peaks located at 425, 449, 482, and ~513 nm were observed. In comparison to the PL spectrum of the PFO solution, the emission maxima of the PFO film were found to be red-shifted and the relative intensities of the (0−2) singlet exciton transition were increased. This was deduced to be caused by increased intermolecular interactions in the solid state.[31] However, in case of the GO-PFO NPs, the emission characteristics of the film were identical to those of the solution state. This indicates that there was no change in the conformation of the PFO chains in the NPs during the film formation process and that chain−chain interactions were limited by particle formation. Furthermore, we confirmed that there was no change in the characteristic green emission of the GO-PFO NPs above 515 nm after film formation.

Until now, the origin of the low-energy green emission of PFO was not fully understood, with two possible mechanisms suggested: the intermolecular aggregates (or excimers) mechanism[32,33] and the keto-defect mechanism.[34] To investigate the formation of the keto defect in GO-PFO NPs, the PFO inside the GO-PFO NPs was selectively redissolved in chloroform and monitored using UV−vis and PL measurements. If such defects were mainly responsible for the green emission, the broad green emission band would be retained after selective redissolution of the PFO. Figure 4a shows photographs of the two-phase solution before and after selective redissolution of the PFO from GO-PFO NPs. Because of the higher density of chloroform (d = 1.483 g/cm^3) in comparison to water, an aqueous layer containing GO-PFO NPs was seen to separate from the chloroform layer. After shaking this two-phase solution, the PFO inside the GO-PFO NPS dissolved in the chloroform (bottom phase). Figure 4b demonstrates that the redissolution of the PFO resulted in complete recovery of its pristine blue emission, with no green emission observed. This indicates that the green emission of the GO-PFO NPs was not caused by keto-defect formation in the PFO.

Second, the optical properties of the GO-PFO NPs were compared to those of PFO NPs prepared in the absence of GO nanosheets. PFO NPs without a GO shell were fabricated by using a typical reprecipitation method (see synthesis procedure in the Methods section). As shown in Figure 3c, the absorption spectrum of the PFO NPs shows a characteristic feature attributed to α-phase domains at around 390 nm,

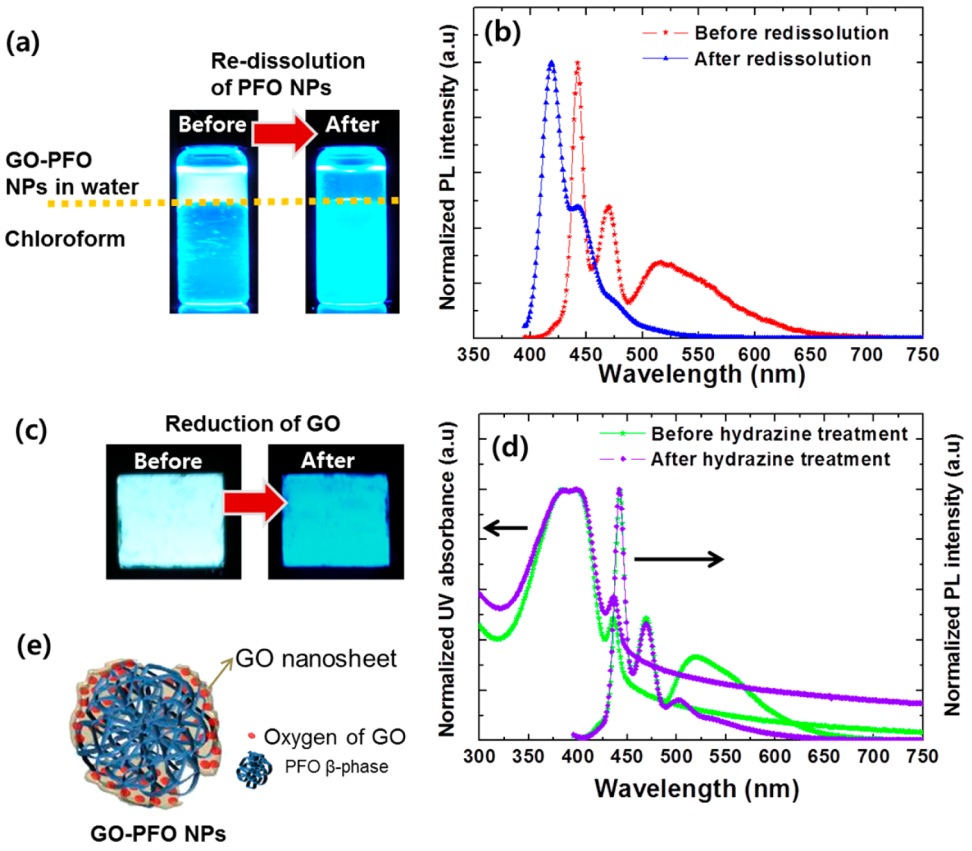

Figure 4. (a) Photographs (λ_{ex} = 365 nm) and (b) PL spectra of a GO-PFO NP solution before and after redissolution of GO-PFO NP into chloroform. (c) Photographs (λ_{ex} = 365 nm) and (d) UV−vis absorption and PL spectra of a GO-PFO NP film before and after reduction of GO. (e) Schematic illustration of GO-PFO NP.

but in a red-shifted position at around 410 nm. A substantial absorption at 439 nm can also be seen, reflecting a small fraction of the planar conformation of PFO (β-phase), which corresponds with previously reported optical properties of PFO NPs.[12] However, it should be noted that no distinct green emission was observed in the PL emission spectra of PFO NPs without GO nanosheets. Additionally, we verified that a solution of GO nanosheets did not exhibit any PL emission under the same excitation conditions (Figure S4). These results imply that the green emission of the GO-PFO NPs was related to the GO nanosheet shell surrounding the PFO NPs and did not originate from the emission of PFO NPs or GO nanosheets in isolation.

To elucidate the mechanism of the effect of the GO nanosheet shell on the emission of GO-PFO NPs, we carried out reduction of the GO nanosheets surrounding the PFO NPs. Reduction of GO is commonly achieved by exposure to hydrazine vapor.[35,36] We verified this method by exposing GO to hydrazine vapor for 2 h, followed by mild thermal annealing at 90 °C, which led to the transformation of GO from an insulator to a semimetal (Figure S5). Figure 4c clearly shows the color change in the PL of the GO-PFO NPs from white to blue on reduction of the GO. When PFO NPs without the GO shell were exposed to the reducing agent, there was no change in the PL, which indicates that the PL change in the presence of GO was mainly due to its reduction. UV−vis absorption and PL spectra of GO-PFO NPs film before and after reduction of GO can be seen in Figure 4d. It is interesting to observe that the broad green emission band above 515 nm significantly decreased in intensity after reduction of GO. This indicates that the presence of oxygen-containing functional groups on the GO nanosheets, such as carboxylic acids, hydroxyl, and epoxide groups, contributed to the low-energy green emission of the GO-PFO NPs. Although the mechanism of this green emission is not clear, it could be suggested that it involved quasi-oxygen doping of the fluorine segment due to interaction with the oxygen-containing groups of GO at the PFO/GO interface. At this location, the quasi-oxygen doping would be reversible and therefore undergo dedoping on reduction of the GO. This is agreement with previous reports where green emissions were observed from polyfluorene derivatives with polar end groups[33] or oxygen-containing side chains,[32] but not from the fluorenone moiety in PFO itself. Quasi-oxygen doping of fluorine by GO can provide a low energy state as deep electron traps,[34,37] which can contribute to the green emission *via* efficient energy transfer. However, further investigation regarding how the oxygen-containing functional groups affect the green emission of GO-PFO NPs is

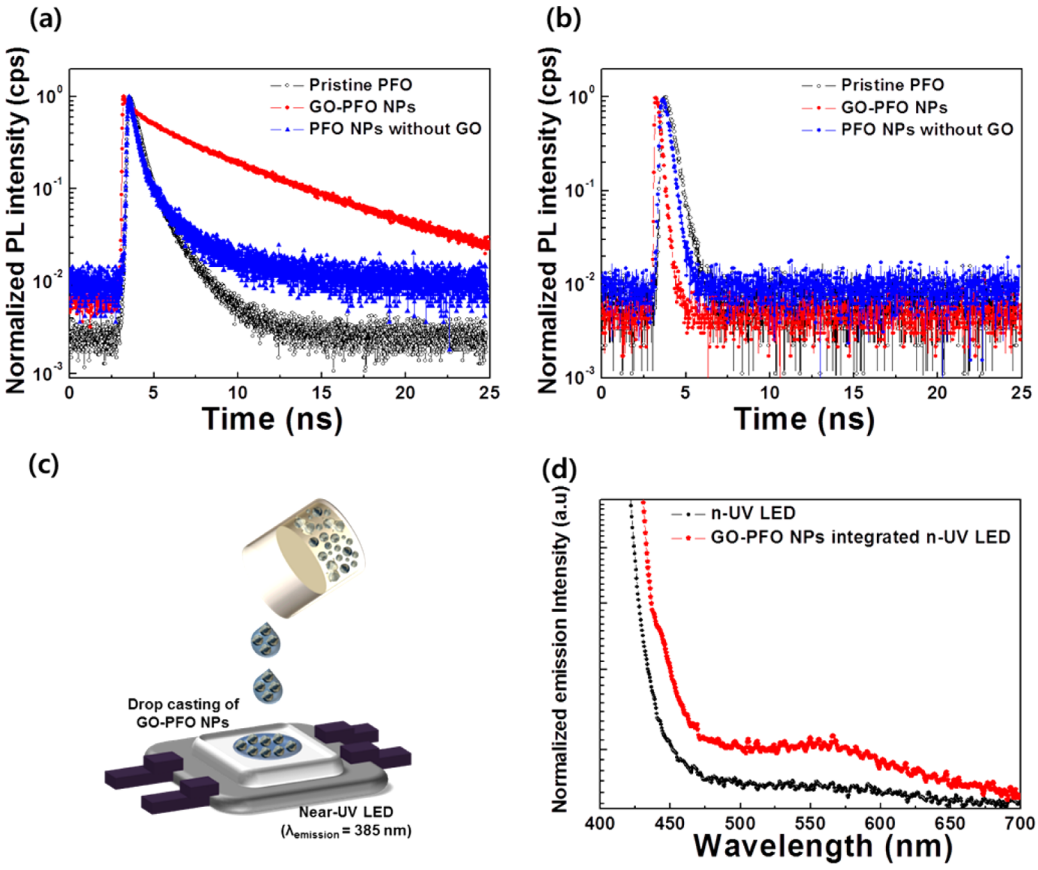

Figure 5. (a) PL decay of PFO, GO-PFO NP, and PFO NP solutions, showing the emission spectrum related to the green broad band emission (550 nm). (b) PL decays at the 0−0 PL emission wavelengths: pristine PFO in chloroform at 420 nm, GO-PFO NP solution at 440 nm, PFO NP solution at 440 nm. (c) Schematic illustration of GO-PFO NP integration into a n-UV LED. (d) Emission spectrum of GO-PFO NPs integrated in n-UV LED electrically driven at 100 mA.

required. We found that there was no green emission when large GO nanosheets (500 nm or 1 μm in a long lateral distance) wrapped several PFO NPs at once or when the relative content of GO to PFO was decreased.

To investigate the quasi-doping effect of the GO-nanosheet shell on other CPNs, we prepared GO nanosheet wrapped CPNs using poly(2-methoxy-5-(2-ethylhexyloxy)-1,4-phenylenevinylene) (MEH-PPV), which is a representative red-emissive polymer with poly(*p*-phenylenevinylene) backbone structure *via* the same emulsification process proposed in this work. UV−vis absorption and PL properties of GO nanosheet wrapped MEH-PPV nanoparticles (GO-MEH PPV NPs) in aqueous solution were compared with those of an MEH PPV NP solution prepared in the absence of GO nanosheets. As shown in Figure S6 of the Supporting Information, the emission features of GO-MEH PPV NPs were not significantly affected by the presence of the GO shell. This result implies that the quasi-doping effect of GO nanosheets is dependent on the conjugated polymer structure, and polyfluorene materials are more strongly influenced by the GO shell compared with the poly(*p*-phenylenevinylene) materials.

Figure 5a shows time-resolved PL decay for the pristine PFO, GO-PFO NPs, and PFO NPs. The excitation wavelength was 385 nm, and the PL decay measurements were taken at a detection wavelength of 550 nm, which corresponds to low-energy green emission. The decay curves were fitted according to the following equation:[38]

$$I(t) = \sum_{i=1}^{n} A_i \exp\left(-\frac{t}{\tau_i}\right)$$

where A_i and τ_i are the pre-exponential factors and the time constants of the different exponentials, respectively. All parameters obtained from the fits are summarized in Table 1. For pristine PFO and PFO NPs the decays were successfully fitted using two exponentials with decay times of 1.66 and 2.34 ns, respectively. In comparison, the PL decay for the GO-PFO NP solution was fitted using three exponentials with slow decay times of 7.09 ns. This indicates that the GO-PFO NPs had much longer PL lifetimes than pristine PFO or PFO NPs. Figure 5b shows single-exponential PL decays of three solutions at the 0−0 PL emission band. In particular, it can be seen that the GO-PFO NPs exhibited a faster decay time of 0.2 ns compared to pristine PFO (0.45 ns) and PFO NPs (0.32 ns). The fast decay of GO-PFO NPs may be related to the energy transfer to a lower energy state, induced by the GO shell. The energy transfer rate can

TABLE 1. Pre-exponential Factors and Decay Time Constants Obtained from the Fits

sample	A_1	τ_1 (ns)	A_2	τ_2 (ns)	A_3	τ_3 (ns)	χ^2
pristine PFO	0.89	0.48	0.11	1.66			1.13
GO-PFO NPs	0.27	0.08	0.26	2.02	0.47	7.09	1.02
PFO NPs	0.90	0.40	0.09	2.34			1.03

be calculated using the following equation (Figure 5c):[38]

$$K_{ET} = \frac{1}{\tau_1}$$

where τ_1 corresponds to the PL decay time at the 0−0 PL emission. The energy transfer rates of pristine PFO, GO-PFO NPs, and PFO NPs were estimated to be 2.2×10^9, 5×10^9, and 3.2×10^9 s^{-1}, respectively. The enhanced energy transfer rate of the PFO NPs without GO compared to pristine PFO chains might be attributed to efficient energy transfer from isolated glassy chains to aggregated β-phase chains with a lower energy state.[27] The more enhanced energy transfer rate of the GO-PFO NPs suggests that the presence of GO nanosheet shells on the PFO NP surface might induce highly efficient energy transfer to the lowest energy state, induced by quasi-doping of the PFO NP surface by the GO.

Fluorescence quantum yields (Φ) of the CPNs were measured in dilute aqueous solutions using quinine sulfate (Φ = 0.55 in 0.1 N H_2SO_4) as a reference. The fluorescence quantum yields for GO-PFO NPs and PFO NPs were determined as 0.03 and 0.05, respectively. Decreased quantum yield of GO-PFO NPs might be due to the fluorescence quenching effect of GO. It is well known that residual graphitic domains within GO quenched fluorescence of nearby fluorescent species including conjugated polymers.[39,40]

Thin films of GO-PFO NPs were evaluated as the color conversion layer of a near-UV light-emitting diode (n-UV LED). The InGaN/GaN multiple quantum well n-UV LED with a peak wavelength of 385 nm was grown on a c-plane sapphire substrate by metal−organic chemical vapor deposition and fabricated by standard microfabrication processes. Thin films of GO-PFO NPs prepared by drop casting were included in the n-UV LED structure, as shown in Figure 5c. The normalized emission spectrum of the GO-PFO NPs excited by the n-UV LED is exhibited in Figure 5d. Even though the peaks at around 440 and 470 nm are not easily resolvable because of the broad full width half-maximum of the LED at the current levels required to pump the nanoparticles, the shoulder around 440 nm and broad band around 550 nm of the resulting spectrum corresponded well with the previously measured PL of the GO-PFO NPs. This demonstrates their potential application for use as a luminophore in lighting applications.

CONCLUSIONS

We have successfully developed novel white-emissive water-dispersible CPNs wrapped by GO nanosheets. Highly stable PFO NPs with diameters in the range 30−150 nm were formed when single-layer GO nanosheets with a small lateral distance of about 200 nm absorbed at the NP oil/water interface, lowering the interfacial tension in the emulsification process. The synthesized GO-PFO NPs exhibited unique white luminescence, which was caused by the presence of a green emission band above 500 nm. It was confirmed that this green emission originated from the existence of the GO nanosheet shell surrounding the PFONPs, not from the luminescence of GO itself or formation of keto defects in the PFO chain. Initiation of the green emission by oxygen-containing functional groups of the GO nanosheet shell suggests that the fluorine chain might be quasi-doped by the oxygen of GO, resulting in the lower energy state responsible for green emission. PL decay analysis confirmed that the GO wrapping of the PFO NPs produces a longer luminescence lifetime than PFO NPs without GO and that highly efficient energy transfer to a lower energy state was induced by the GO. Finally we prepared a proof-of-concept GO-PFO NP integrated color-conversion UV-LED, which demonstrates the potential of these particles for use in lighting applications. We believe that this work provides a new strategy for the synthesis of graphene-wrapped nanomateirals for a variety of applications such as optoelectronic devices, sensors, and bioimaging systems.

METHODS

Materials. Poly(9,9-di-*n*-octylfluorenyl-2,7-diyl) (average MW = 58 200; polydispersity = 3.7), chloroform (anhydrous, 99.9%), tetrahydrofuran (THF), H_2SO_4 (98%), aqueous NH_3 (28%), and hydrazine (35%) were purchased from Sigma-Aldrich. Deionized water (18.3 MΩ) was used throughout the experiments. Expandable graphite (natural grade, ~100 mesh, 99.9% with metals basis) was purchased from Asbury Graphite Mills and used as received. $KMnO_4$ and 30% H_2O_2 aqueous solution were obtained from Yakuri. All chemicals were used without further purification.

Preparation of GO Nanosheets. The GO was prepared *via* the modified Hummers method using expandable graphite flake as a starting material. The expandable graphite flakes (~0.85 g) were ground using a ball mill and then stirred in 98% H_2SO_4 (23 mL) for 8 h. $KMnO_4$ (3 g) was gradually added to this mixture while keeping the temperature below 20 °C. The mixture was then stirred at 36 °C for 30 min, at 70 °C for 45 min, and finally at 100 °C for 30 min after adding water (140 mL). After termination of the reaction by addition of 30% H_2O_2 solution (10 mL), the products were washed by centrifugation twice with a 5% HCl aqueous solution and twice with water. The synthesized graphite oxide was suspended in water to give a brown dispersion, which was subjected to dialysis to completely remove residual salts and acids. The purified mixture was diluted to a final

volume of 1.5 L with water. Exfoliation of graphite oxide to GO was achieved by ultrasonication for 30 min and then centrifugation for 30 min to remove any unexfoliated graphite oxide. This gave GO sheets with a wide range of lateral dimensions from a few hundreds of nanometers to several micrometers.

To wrap the individual polymer particles with GO, the average lateral size of the GO should be reduced. A 0.02 wt % GO solution (20 mL) and 70% HNO_3 solution (10 mL) were mixed and then ultrasonicated at 60 °C for 4 h to reduce the average lateral size of GO. The mixture was poured into distilled water (400 mL) and then was subjected to dialysis for a week to remove residual acid. The final GO nanosheets were characterized and used in the subsequent wrapping step.

Preparation of Polymer NPs Wrapped with GO Nanosheets. The PFO polymer was added to chloroform with a concentration of 10.0 mg/mL and left to dissolve for 1 day under N_2 in a glovebox. The solution was then filtered through a 0.2 μm poly(tetrafluoroethylene) filter. The polymer solution (1 mL) was injected into an aqueous solution of GO (10 mL). This two-phase solution was then emulsified using a tip sonicator (30 W, 4 min). The dispersion was vigorously stirred on a hot plate at 60 °C to evaporate the remaining $CHCl_3$ present in the solution. Thin films of the obtained GO-PFO NPs were then prepared by drop-casting the solution onto a glass substrate, followed by drying in a vacuum oven.

Preparation of PFO NPs without GO. A solution of the conjugated polymer in THF (2.0 mg/mL) was prepared under a N_2 environment in a glovebox. One milliliter of this was then rapidly injected into deionized water (10 mL) at 45 °C with sonication. The THF was removed by partial vacuum evaporation; then the final solution was filtered through a 2.7 μm syringe filter before further characterization.

Fabrication of near-UV LED (n-UV LED) Device. GaInN/GaN multiple quantum well n-UV LED wafers were grown on a c-plane sapphire substrate by metal−organic chemical vapor deposition. A 2.5 μm thick unintentionally doped GaN was grown, followed by the growth of a 3 μm thick Si-doped n-type GaN layer, a five-period 3 nm thick GaInN well with 5 nm thick GaN barriers, a 20 nm p-type AlGaN layer, and a 0.2 μm p-type GaN layer. The n-UV LED wafer was processed into 300 × 300 μm^2 lateral-structure devices. The LED mesa structures were obtained by photolithographic patterning followed by inductively coupled plasma reactive-ion etching with BCl3/Cl2 gas. Subsequently, Ti/Al n-type ohmic contacts were deposited on the exposed n-type GaN by electron-beam evaporation and annealed at 650 °C for 1 min in N_2 ambient. Ni/Au (5/5 nm) p-type ohmic contacts were deposited on the mesa and annealed at 500 °C for 1 min in air ambient, followed by the deposition of Ti/Au pad metal.

Analysis. The synthesized GO-PFO NPs were visualized with a field emission scanning electron microscope (FE-SEM, Hitachi S-4100) at a maximum accelerating voltage of 10 kV. The ultraviolet−visible (UV−vis) absorption spectra were measured with an Agilent 8453. The photoluminescence characteristics of the materials were collected on a Hitachi F-7000. The size distribution of GO-PFO NPs was characterized by dynamic light scattering (ELS-Z2, Otuska Electronic). All of the particle size measurements were conducted on 0.1 mg/mL aqueous dispersions. The samples for transmission electron microscopy were prepared by drop-casting 3 μL aliquots of the solution onto a carbon-coated copper grid, which was subsequently placed on a piece of paper to get rid of excess solvent. The samples were then left to dry for 6 h to form a thin film. The images were obtained on a JEM-3100 microscope operating at 200 or 300 kV accelerating voltage, using images acquired with an ORIUS-SC 600 CCD camera (Gatan, Inc.) as a base point. Cryogenic-transmission electron microscopy was performed with a thin film of solution (5 μL) transferred to a lacey supported grid (Ted Pella). The thin solution films were prepared under controlled temperature and humidity conditions within a custom-built environmental chamber in order to prevent evaporation of solvent from sample solution. The excess liquid was blotted with filter paper for 1−2 s, and the thin aqueous films were rapidly vitrified by plunging them into liquid ethane. The grid was transferred to a Gatan 626 cryoholder, using a cryo-transfer device, and then placed in a JEM-2010. Direct imaging was carried out at a temperature of approximately −175 °C and with a 200 kV accelerating voltage, using the images acquired with a SC 1000 CCD camera and processed with Digital Micrograph (Gatan, Inc., Warrendale, PA, USA). PL lifetime decays were measured using an inverted-type scanning confocal microscope (MicroTime-200, Picoquant, Germany) with a 60× objective. A single-mode pulsed diode laser (375 nm with a pulse width of ~240 ps at full width at half-maximum) was used as an excitation source. A dichroic mirror (Z375RDC, AHF), a long-pass filter (HQ405lp, AHF), and an avalanche photodiode detector (PDM series, MPD) were used to collect emission from the film samples. Time-correlated single-photon counting was used to count emission photons, and the obtained decay curves were fitted by a two-exponential fitting model to evaluate the PL lifetimes.

Conflict of Interest: The authors declare no competing financial interest.

Acknowledgment. This work was supported by the Korea Institute of Science and Technology (KIST) Future Resource Research Program (2E24011) and the Global Frontier Research Program by the Ministry of Education, Science and Technology (2011-0032155). The authors thank Dr. Weon-Sik Chae, KBSI, for the PL lifetime measurements.

Supporting Information Available: This material is available free of charge *via* the Internet at http://pubs.acs.org.

Note Added after ASAP Publication: This paper was published ASAP on April 15, 2014. Affiliations for authors N.D.K.T., H.K., and J.A.L. were updated, and the revised version was reposted on April 18, 2014.

REFERENCES AND NOTES

1. Huebner, C. F.; Roeder, R. D.; Foulger, S. H. Nanoparticle Electroluminescence: Controlling Emission Color through Forster Resonance Energy Transfer in Hybrid Particles. *Adv. Funct. Mater.* **2009**, *19*, 3604–3609.
2. Fisslthaler, E.; Blumel, A.; Landfester, K.; Scherf, U.; List, E. J. W. Printing Functional Nanostructures: a Novel Route towards Nanostructuring of Organic Electronic Devices *via* Soft Embossing, Inkjet Printing and Colloidal Self Assembly of Semiconducting Polymer Nanospheres. *Soft Matter.* **2008**, *4*, 2448–2453.
3. Tuncel, D.; Demir, H. V. Conjugated Polymer Nanoparticles. *Nanoscale* **2010**, *2*, 484–494.
4. Kaeser, A.; Schenning, A. P. H. J. Fluorescent Nanoparticles Based on Self-Assembled pi-Conjugated Systems. *Adv. Mater.* **2010**, *22*, 2985–2997.
5. DiMaio, J. R.; Kokuoz, B.; Ballato, J. White Light Emissions through Down-Conversion of Rare-Earth Doped LaF_3 Nanoparticles. *Opt. Express* **2006**, *14*, 11412–11417.
6. Hsu, C. Y.; Liu, Y. L. Rhodamine B-Anchored Silica Nanoparticles Displaying White-Light Photoluminescence and Their Uses in Preparations of Photoluminescent Polymeric Films and Nanofibers. *J. Colloid Interface Sci.* **2010**, *350*, 75–82.
7. Malinge, J.; Allain, C.; Brosseau, A.; Audebert, P. White Fluorescence from Core-Shell Silica Nanoparticles. *Angew. Chem., Int. Ed.* **2012**, *51*, 8534–8537.
8. Son, D. I.; Kwon, B. W.; Park, D. H.; Seo, W. S.; Yi, Y.; Angadi, B.; Lee, C. L.; Choi, W. K. Emissive ZnO-Graphene Quantum Dots for White-Light-Emitting Diodes. *Nat. Nanotechnol.* **2012**, *7*, 465–471.
9. Vijayakumar, C.; Sugiyasu, K.; Takeuchi, M. Oligofluorene-Based Electrophoretic Nanoparticles in Aqueous Medium as a Donor Scaffold for Fluorescence Resonance Energy Transfer and White-Light Emission. *Chem. Sci.* **2011**, *2*, 291–294.
10. Park, E. J.; Erdem, T.; Ibrahimova, V.; Nizamoglu, S.; Demir, H. V.; Tuncel, D. White-Emitting Conjugated Polymer Nanoparticles with Cross-Linked Shell for Mechanical Stability and Controllable Photometric Properties in Color-Conversion LED Applications. *ACS Nano* **2011**, *5*, 2483–2492.

11. Landfester, K.; Montenegro, R.; Scherf, U.; Guntner, R.; Asawapirom, U.; Patil, S.; Neher, D.; Kietzke, T. Semiconducting Polymer Nanospheres in Aqueous Dispersion Prepared by a Miniemulsion Process. *Adv. Mater.* **2002**, *14*, 651–655.
12. Huebner, C. F.; Foulger, S. H. Spectral Tuning of Conjugated Polymer Colloid Light-Emitting Diodes. *Langmuir* **2010**, *26*, 2945–2950.
13. Eda, G.; Chhowalla, M. Chemically Derived Graphene Oxide: Towards Large-Area Thin-Film Electronics and Optoelectronics. *Adv. Mater.* **2010**, *22*, 2392–2415.
14. Kim, J.; Cote, L. J.; Kim, F.; Yuan, W.; Shull, K. R.; Huang, J. X. Graphene Oxide Sheets at Interfaces. *J. Am. Chem. Soc.* **2010**, *132*, 8180–8186.
15. Zhang, F. F.; Zhang, X. B.; Dong, Y. H.; Wang, L. M. Facile and Effective Synthesis of Reduced Graphene Oxide Encapsulated Sulfur *via* Oil/Water System for High Performance Lithium Sulfur Cells. *J. Mater. Chem.* **2012**, *22*, 11452–11454.
16. Chen, Y. T.; Guo, F.; Jachak, A.; Kim, S. P.; Datta, D.; Liu, J. Y.; Kulaots, I.; Vaslet, C.; Jang, H. D.; Huang, J. X.; *et al*. Aerosol Synthesis of Cargo-Filled Graphene Nanosacks. *Nano Lett.* **2012**, *12*, 1996–2002.
17. Yang, S. B.; Feng, X. L.; Ivanovici, S.; Mullen, K. Fabrication of Graphene-Encapsulated Oxide Nanoparticles: Towards High-Performance Anode Materials for Lithium Storage. *Angew. Chem., Int. Ed.* **2010**, *49*, 8408–8411.
18. Cassagneau, T.; Fendler, J. H. Preparation and Layer-By-Layer Self-Assembly of Silver Nanoparticles Capped by Graphite Oxide Nanosheets. *J. Phys. Chem. B* **1999**, *103*, 1789–1793.
19. Zhou, W. W.; Zhu, J. X.; Cheng, C. W.; Liu, J. P.; Yang, H. P.; Cong, C. X.; Guan, C.; Jia, X. T.; Fan, H. J.; Yan, Q. Y.; *et al*. A General Strategy Toward Graphene@Metal Oxide Core-Shell Nanostructures for High-Performance Lithium Storage. *Energy Environ. Sci.* **2011**, *4*, 4954–4961.
20. Han, T. H.; Lee, W. J.; Lee, D. H.; Kim, J. E.; Choi, E. Y.; Kim, S. O. Peptide/Graphene Hybrid Assembly into Core/Shell Nanowires. *Adv. Mater.* **2010**, *22*, 2060–2064.
21. Akhavan, O.; Ghaderi, E.; Esfandiar, A. Wrapping Bacteria by Graphene Nanosheets for Isolation from Environment, Reactivation by Sonication, and Inactivation by Near-Infrared Irradiation. *J. Phys. Chem. B* **2011**, *115*, 6279–6288.
22. Mohanty, N.; Fahrenholtz, M.; Nagaraja, A.; Boyle, D.; Berry, V. Impermeable Graphenic Encasement of Bacteria. *Nano Lett.* **2011**, *11*, 1270–1275.
23. Zeng, Q. C.; Wu, D. C.; Zou, C.; Xu, F.; Fu, R. W.; Li, Z. H.; Lianga, Y. R.; Su, D. S. Template-Free Fabrication of Hierarchical Porous Carbon Based on Intra-/Inter-Sphere Crosslinking of Monodisperse Styrene-Divinylbenzene Copolymer Nanospheres. *Chem. Commun.* **2010**, *46*, 5927–5929.
24. Wilson, N. R.; Pandey, P. A.; Beanland, R.; Young, R. J.; Kinloch, I. A.; Gong, L.; Liu, Z.; Suenaga, K.; Rourke, J. P.; York, S. J.; *et al*. Graphene Oxide: Structural Analysis and Application as a Highly Transparent Support for Electron Microscopy. *ACS Nano* **2009**, *3*, 2547–2556.
25. Jeong, H. K.; Lee, Y. P.; Lahaye, R. J. W. E.; Park, M. H.; An, K. H.; Kim, I. J.; Yang, C. W.; Park, C. Y.; Ruoff, R. S.; Lee, Y. H. Evidence of Graphitic AB Stacking Order of Graphite Oxides. *J. Am. Chem. Soc.* **2008**, *130*, 1362–1366.
26. Meyer, J. C.; Geim, A. K.; Katsnelson, M. I.; Novoselov, K. S.; Obergfell, D.; Roth, S.; Girit, C.; Zettl, A. On the Roughness of Single- and Bi-Layer Graphene Membranes. *Solid State Commun.* **2007**, *143*, 101–109.
27. Wu, C. F.; McNeill, J. Swelling-Controlled Polymer Phase and Fluorescence Properties of Polyfluorene Nanoparticles. *Langmuir* **2008**, *24*, 5855–5861.
28. Grell, M.; Bradley, D. D. C.; Ungar, G.; Hill, J.; Whitehead, K. S. Interplay of Physical Structure and Photophysics for a Liquid Crystalline Polyfluorene. *Macromolecules* **1999**, *32*, 5810–5817.
29. Asada, K.; Kobayasi, T.; Naito, H. Control of Effective Conjugation Length in Polyfluorene Thin Films. *Jpn. J. Appl. Phys. Part 2* **2006**, *45*, L247–L249.
30. Liu, S. J.; Xu, W. J.; Ma, T. C.; Zhao, Q.; Fan, Q. L.; Ling, Q. D.; Huang, W. Effects of Temperature and Solvent on the Energy Transfer and beta-Phase Formation in the Iridium(III) Complex-Containing Polyfluorene in Solutions and as Suspended Nano-Particles. *Macromol. Rapid Commun.* **2010**, *31*, 629–633.
31. Charas, A.; Morgado, J.; Martinho, J. M. G.; Fedorov, A.; Alcacer, L.; Cacialli, F. Excitation Energy Transfer and Spatial Exciton Confinement in Polyfluorene Blends for Application in Light-Emitting Diodes. *J. Mater. Chem.* **2002**, *12*, 3523–3527.
32. Koizumi, Y.; Seki, S.; Tsukuda, S.; Sakamoto, S.; Tagawa, S. Self-Condensed Nanoparticles of Oligofluorenes with Water-Soluble Side Chains. *J. Am. Chem. Soc.* **2006**, *128*, 9036–9037.
33. Chen, X. W.; Tseng, H. E.; Liao, J. L.; Chen, S. A. Green Emission from End-Group-Enhanced Aggregation in Polydioethylfluorene. *J. Phys. Chem. B* **2005**, *109*, 17496–17502.
34. Romaner, L.; Pogantsch, A.; de Freitas, P. S.; Scherf, U.; Gaal, M.; Zojer, E.; List, E. J. W. The Origin of Green Emission in Polyfluorene-Based Conjugated Polymers: On-Chain Defect Fluorescence. *Adv. Funct. Mater.* **2003**, *13*, 597–601.
35. Eda, G.; Fanchini, G.; Chhowalla, M. Large-Area Ultrathin Films of Reduced Graphene Oxide as a Transparent and Flexible Electronic Material. *Nat. Nanotechnol.* **2008**, *3*, 270–274.
36. Shin, K. Y.; Hong, J. Y.; Jang, J. Micropatterning of Graphene Sheets by Inkjet Printing and Its Wideband Dipole-Antenna Application. *Adv. Mater.* **2011**, *23*, 2113–2118.
37. Zhou, X. H.; Zhang, Y.; Xie, Y. Q.; Cao, Y.; Pei, J. Effect of Fluorenone Units on the Property of Polyfluorene and Oligofluorene Derivatives: Synthesis, Structure-Properties Relationship, and Electroluminescence. *Macromolecules* **2006**, *39*, 3830–3840.
38. Fakis, M.; Anestopoulos, D.; Giannetas, V.; Persephonis, P.; Mikroyannidis, J. Femtosecond Time Resolved Fluorescence Dynamics of a Cationic Water-Soluble Poly(fluorenevinylene-co-phenylenevinylene). *J. Phys. Chem. B* **2006**, *110*, 12926–12931.
39. Kim, J.; Cote, L. J.; Kim, F.; Huang, J. X. Visualizing Graphene Based Sheets by Fluorescence Quenching Microscopy. *J. Am. Chem. Soc.* **2010**, *132*, 260–267.
40. Liu, Z. F.; Liu, Q.; Huang, Y.; Ma, Y. F.; Yin, S. G.; Zhang, X. Y.; Sun, W.; Chen, Y. S. Organic Photovoltaic Devices Based on a Novel Acceptor Material: Graphene. *Adv. Mater.* **2008**, *20*, 3924–3930.